PARTICLE SIMULATION OF THE RESISTIVE G-MODE IN A SHEARED MAGNETIC FIELD

R.D. Sydora, J.N. Leboeuf, P.H. Diamond, Z.G. An, and T. Tajima

Institute for Fusion Studies
The University of Texas at Austin
Austin, Texas 78712

ABSTRACT

The linear and nonlinear evolution of the interchange instability of a resistive plasma (the resistive g-mode) in a sheared magnetic field is studied using electrostatic particle simulation methods. Both the fast and slow interchange mode regimes are considered. In both cases the linear growth rates of the modes scale well with the theoretical values. The saturation of the instabilities is due primarily to convective mixing of pressure over the width of the eigenmode. The saturation levels predicted by mixing length theory are in reasonable agreement with the simulation results.

I. INTRODUCTION

The resistive interchange mode can cause significant anomalous particle and heat transport across the magnetic field in a plasma of such devices as the reversed field pinch[1] (RFP), spheromak,[2] and other possible situations. Study of resistive g-mode stability and associated transport is important for the RFP since it is a relatively high beta device relying on strong magnetic shear rather than average minimum-B for the stabilization of localized modes. Resistive interchange modes cannot be stabilized by either shear or conducting walls alone. When they appear, magnetic islands can form and this may result in enhanced thermal conduction losses. Thus it is possible that the limiting plasma beta in the RFP may be determined by the nonlinear g-mode behavior.

In this paper we investigate the linear and nonlinear evolution of the resistive g-mode using electrostatic particle simulation methods. This is applicable to a regime of large collisionality and low beta. This electrostatic model, in the appropriate regime, still allows us to consider kinetic modifications to the modes, such as diamagnetic and finite Larmor radius effects, which can alter the scaling of the growth rate versus resistivity. We also consider the two interchange mode growth regimes, the fast and slow.[3] The fast interchange mode growth rate corresponds to that of the Rayleigh-Taylor instability, which is independent of the magnetic field strength and resistivity. The slow interchange mode growth rate varies as one-third the power of the resistivity. Since the modes we will consider are localized with radial extent of approximately a few ion gyroradii, the modes with the

slow growth rate are of more physical relevance to experimental devices.

There has been extensive theoretical and numerical work on the resistive interchange mode. A great deal of the theoretical work has been to determine stability properties of g-modes with the inclusion of finite Larmor radius effects,[4,5] parallel ion viscosity,[6] temperature gradients,[7] and diamagnetic effects.[8] Previous simulation work has centered on determining the gross plasma motion and saturation levels for interchange modes in diffuse pinches.[9-11] Hender and Robinson[12] and An and Diamond[13] have recently studied the nonlinear evolution of the resistive g-mode and the associated anomalous energy transport. Experimentally, the resistive g-mode has been observed in Levitron experiments at Culham[14] and is thought to be a cause of the magnetic field fluctuations measured in the HBTX-I reversed field pinch.[15]

The reasons particle simulation methods are uniquely suited to investigate the evolution of the resistive g-mode are listed as follows. First, the stability of short wavelength modes ($k_\perp \rho_s \gtrsim 1$) can be determined. Second, when multi-rational surfaces are introduced and overlapping magnetic islands are present, the regime $L < v_e/\nu_{ei}$, where L is the parallel stochastic magnetic field decorrelation length, $v_e = (T_e/m_e)^{1/2}$ is the electron thermal velocity and ν_{ei} is the electron-ion collision frequency, can be studied. This allows one to validate stochastic magnetic field line calculations of heat transport as well as investigate possible anomalous electron viscosity. However, before undertaking these problems, the electrostatic model is used to verify the linear theory of resistive g-modes and determine the saturation mechanism.

The organization of this paper is as follows. In Sec. II the simulation model and initial configuration is presented. In Sec. III the linear theory of the resistive interchange mode is reviewed and simulation results presented for the fast and slow interchange mode growth rates as well as a comparison with linear theory. In Sec. IV the saturation mechanism of the unstable resistive g-mode is given as well as a comparison of the predicted values with the simulation results. Section V contains the discussion and conclusions.

II. SIMULATION MODEL AND CONFIGURATION

We consider the plane slab model of Furth, Killeen, and Rosenbluth[4] of an incompressible fluid in which the destabilizing effect of magnetic field curvature is represented by an effective gravitational field. In the plane slab model the equilibrium magnetic field lies in the (y,z) plane and is given by $\underset{\sim}{B} = (0, B_o x/L_s, B_o)$ as shown in Fig. 1. To relate to a cylindrical plasma column, the x-axis may be regarded as the radial coordinate with $x = r-r_o$, where r_o is the position of the mode rational surface. Therefore, the wavenumber along the magnetic field, $k_\parallel$, is given by $k_\parallel = \underset{\sim}{k}\cdot\underset{\sim}{B}/|\underset{\sim}{B}| \simeq k_y(r-r_o)/L_s$ with $k_y = 2\pi m/L_y$, $m=0, \pm1, \ldots, \pm L_y/2$. The density is assumed to vary radially and the profile used initially is

$$n(x) = n_o \kappa L_x \left[e^{-\kappa x}/\left(1 - e^{-\kappa L_x}\right)\right] , \qquad (1)$$

which gives a constant density gradient scale length, L_n ($\equiv -1/\kappa$ where $\kappa = -n'(x)/n(x)$), where L_x is the system length in the x-direction. No gradients in temperature are imposed.

In order to simulate magnetic field curvature, we introduce a gravitational field in a direction opposite to the density gradient. The gravitational acceleration is defined as

$$\underset{\sim}{g} = \frac{m(v_{\parallel}^2 + v_{\perp}^2/2)}{L_c} \hat{e}_x \ , \tag{2}$$

where L_c is the curvature scale length and this produces the curvature drift of charged particles. We consider the case of a constant centrifugal force only.

The model used for the particle simulation is a two-and-one-half dimensional (x-y spatial dimension with v_x-v_y-v_z velocity dimension) guiding center electrostatic particle code.[16] The plasma is confined between two boundaries located at x=0 and x=L_x. The system is periodic in the y-direction with length L_y. The boundary condition imposed on the electrostatic potential at the endpoints x=0 and x=L_x is such that the normal component of the electric field vanishes, which requires $\frac{\partial \phi}{\partial x}(x=0) = 0 = \frac{\partial \phi}{\partial x}(x=L_x)$. The parity of the eigenmodes in the simulation is determined by the position of the rational surface relative to the endpoints. For the present situation, with the rational surface at x=0, the parity of the eigenmode will be even with respect to the rational surface using the above boundary conditions.

The particle motion of the electrons in the plane perpendicular to the magnetic field is determined by guiding center equations and ion orbits are followed using the Lorentz force equation. Particles are elastically reflected from the boundaries in the x-direction. In order to include a finite electron-ion collision frequency, a Monte-Carlo

collision operator is used which correctly simulates small-angle collisions and models the Lorentz collision operator.[17] This particular operator gives a Spitzer value for the resistivity.

Since we must consider modes which satisfy $k_x > k_y$ where $k_x \sim 1/\Delta$, and Δ is the approximate radial width of the eigenfunction, it is necessary to make the system extent in the y-direction as long as possible. One method used to achieve this is to expand the electrostatic potential in the y-direction as a sum of normal modes:[18]

$$\phi(x,y) = \sum_{m=-N}^{N} \phi_m(x)\, e^{-ik_y y_j} \,, \tag{3}$$

where y_j is the particle position in the y-direction. This allows the use of very large system lengths and avoids problems associated with grid interpolations in the y-dimension. Generally, only the first few long wavelength modes need to be retained in order to give an accurate representation of the electrostatic potential.

III. LINEAR THEORY AND SIMULATION RESULTS

In this section we briefly review the linear theory of the resistive g-mode and discuss the particle simulation results for fast and slow interchange mode growth rates. The resistive g-mode is localized around the resonant surface, $\underset{\sim}{k}\cdot\underset{\sim}{B} = 0$, which is the position where motion of the fluid and field can most easily decouple. This can be seen from Ohm's law:

$$\underset{\sim}{E} + \frac{\underset{\sim}{v}\times\underset{\sim}{B}}{c} = \eta\underset{\sim}{J} \,, \tag{4}$$

where η is the resistivity. In the extreme collisional case where the fluid moves freely across the field lines, the induced electric field $\underset{\sim}{E} \simeq 0$ near the resonant surface and the z-component of the current in slab geometry is

$$J_z = \frac{x}{L_s} \frac{B}{c} \frac{v_x}{\eta} , \tag{5}$$

where L_s is the shear length of the magnetic field. Therefore, the restraining force exerted on the plasma is given by

$$\underset{\sim}{F} = \frac{\underset{\sim}{J} \times \underset{\sim}{B}}{c} = - \left(\frac{Bx}{cL_s}\right)^2 \frac{v_x}{\eta} \hat{e}_x , \tag{6}$$

and for $x > 0$ and η small the force is very large, which means the plasma cannot slip across the field lines. However, for $x \simeq 0$, corresponding to $\underset{\sim}{k} \cdot \underset{\sim}{B} = 0$, the restraining force is small and the plasma can slip through the field, thereby localizing the mode. It is important to note that the resistive g-mode is dominantly electrostatic.

To describe the linear properties of the resistive g-mode we begin by assuming that the electrons obey a drift-kinetic equation with a number conserving Krook operator used to model the electron-ion collisions. This form of the collision operator gives reasonably accurate results if electron temperature gradients and energy-dependent curvature drifts are neglected.[7] If the linear Vlasov response is used for the ions, the quasineutrality condition leads to the following eigenmode equation:[7]

$$\rho_s^2\left(\frac{\partial^2}{\partial x^2} - k_y^2\right)\phi + \left[-\frac{\omega_* \omega_D \left(\frac{T_i}{T_e} + 1\right)}{(\omega-\omega_{*i})(\omega-\omega_D)} + \frac{\omega(\omega-\omega_*)}{(\omega-\omega_{*i})(\omega-\omega_D)^2}\frac{k_y^2 v_e^2 x^2}{i\nu_{ei}L_s^2}\right]\phi = 0 \ , \qquad (7)$$

where $\rho_s = \sqrt{T_e/T_i}\ \rho_i$, $v_e = (T_e/m_e)^{1/2}$, $\omega_* = k_y c T_e/L_n eB$, $\omega_{*i} = -\omega_* T_i/T_e$, and $\omega_D = k_y c T_e/L_c eB$. The fast and slow interchange mode growth rates can now be derived from this differential equation. To obtain the growth rate of the fast interchange mode, we let $k_y > k_x$, $\omega \simeq i\gamma >> \omega_*$ and the growth rate is[19]

$$\gamma = -\frac{1}{2}\left(\frac{v_e^2 x^2}{\rho_s^2 \nu_{ei} L_s^2}\right) + \left[\frac{1}{4}\left(\frac{v_e^2 x^2}{\rho_s^2 \nu_{ei} L_s^2}\right)^2 + \left(\frac{T_e+T_i}{m_i L_n L_c}\right)\right]^{1/2} \ , \qquad (8)$$

which is independent of the magnetic field strength. When the resistive terms are small the usual Rayleigh-Taylor instability growth rate is found. For the slow interchange mode, $k_x > k_y$, and assuming an eigenfunction of the form

$$\hat{\phi} = e^{-\alpha x^2/2} \ , \ \mathrm{Re}(\alpha) > 0$$

in Eq. (7), we obtain the dispersion relation

$$\omega(\omega - \omega_{*i})(\omega - \omega_*) = -i\gamma_o^3 \ , \qquad (9)$$

where

$$\gamma_o = \left(1 + \frac{T_i}{T_e}\right)^{2/3} \left(\frac{L_s}{L_n}\right)^{2/3} \left(\frac{L_n}{L_c}\right)^{2/3} \left(\frac{m_e}{m_i}\right)^{1/3} \left(\frac{\nu_{ei}}{\omega_*}\right)^{1/3} . \qquad (10)$$

Three limiting cases are considered. For $\omega << \omega_{*i} = -\omega_*$,

$$-i\omega = \frac{\gamma_o^3}{\omega_*^2} \propto \nu_{ei} ; \qquad (11)$$

in the limit $\omega_{*i} < \omega < \omega_*$, it is found that

$$-i\omega = \left(\frac{\gamma_o^3}{2\omega_*}\right)^{1/2} \propto \nu_{ei}^{1/2} ; \qquad (12)$$

and finally, for $\omega >> \omega_{*i} = -\omega_*$,

$$-i\omega = \gamma_o \propto \nu_{ei}^{1/3} . \qquad (13)$$

Therefore, kinetic effects can substantially alter the growth rate scaling with resistivity.

In this paper we only consider the limit of $\omega > \omega_*$, which gives a growth rate of the resistive g-mode proportional to one-third the power of the resistivity. This is the current operating regime of most experimental devices which exhibit resistive interchange mode activity, and diamagnetic drift corrections do not substantially alter our main conclusions. In the next two subsections the particle simulation results of the evolution of resistive interchange modes localized about a single rational surface are presented.

A. Fast interchange mode

In this section the simulation results of the fast interchange mode in a strongly sheared magnetic field are discussed. In order to obtain the fast interchange mode growth we require $k_y > k_x$ and the interchange term in Eq. (7) be much larger than the resistive term. Therefore, the parameters used are listed as follows: $L_x \times L_y = 64\delta \times 64\delta$; $T_e/T_i = 1$; $m_e/m_i = 0.01$; $\omega_{ce}/\omega_{pe} = 10$; $L_s/L_n = 14$; $L_n/L_c = 0.1$; $v_e = 1.4\omega_{pe}\delta$; $a_x = a_y = 1.5\delta$; $\omega_{pe}\Delta t = 2$; $n_o = 16/\delta^2$; and $k_y\rho_s = 0.13m$, $m=0, \pm1, \ldots, \pm L_y/2$. The collision frequency is $\nu_{ei}/\omega_* = 20$ and the rational surface position is located at x=0. Only eigenmodes of even parity with respect to the rational surface are allowed in the system.

In this case several long wavelength modes were observed to grow exponentially at the fast interchange growth rate given by Eq. (8), and then saturated at a later time. Figure 2 illustrates the measured growth rates as a function of wavenumber and the theoretical values obtained from Eq. (8) are also given on the same figure. The electron and ion density profiles are observed to flatten near the mode rational surface and this reduces the gradient in density, which drives the instability. The strong shear localizes the influence of the unstable modes and in Fig. 3 contours of the electrostatic potential at $\omega_{pe}t = 1600$ are shown. The mode localization is clearly visible as well as the unstable wavelength, $k_y\rho_s = 0.39$. The fluctuation levels of various modes at saturation is illustrated in Fig. 4 and $|e\phi/T_e|_{max} \simeq 0.15$, decreasing slightly for the shorter wavelengths.

B. Slow interchange mode

The simulation results using the slow interchange mode ordering are presented in this section. In order to satisfy $k_x > k_y$, the parameters used for this case are: $L_x \times L_y = 32\delta \times 1280\delta$; $T_e/T_i = 1$; $m_e/m_i = 0.01$; $\omega_{ce}/\omega_{pe} = 10$; $L_s/L_n = 28$; $L_n/L_c = 0.016$; $a_x = 1.5\delta$; $a_y = 35\delta$; $v_e = 2.5\omega_{pe}\delta$; $\omega_{pe}\Delta t = 2$; $L_n = 14.28\delta$; and $k_y\rho_s = 0.012m$, m=0, ±1, ±2, ±3. Only six modes were retained in order to satisfy the slow interchange mode condition, $k_x > k_y$. To verify that shear has a strong stabilizing effect on the slow interchange modes over the time scale of the particle simulation runs (several drift periods) we first considered the collisionless limit as a check of the model. The results, using the above parameters, indicated no observable growth rates and the density and temperature profiles remained the same as their initial values over the entire length of the run.

Next, the effects of finite resistivity are included and, using $\nu_{ei}/\omega_* = 50$ with the above parameters, the time evolution of the electron and ion density profiles are shown in Fig. 5. A flattening of the density profiles occurs in a localized region about the mode rational surface. The width of the most unstable eigenmode, $k_y\rho_s = 0.036$, is also included in this figure (Δ) and was determined by a solution to the eigenmode Eq. (7) using a standard shooting code technique. The wave function is illustrated in Fig. 6 along with the mode half width, Δ, for $\nu_{ei}/\omega_* = 50$. Therefore, it is clear that the density relaxation occurs approximately over the width of the eigenmode.

In order to verify the growth rate scaling with resistivity for the slow interchange mode ordering, several simulations were performed keeping the above parameters fixed and varying the resistivity. The results are shown in Fig. 7, which represents the growth rate of the most unstable mode versus resistivity to the one-third power. The simulation results obey the scaling law predicted by linear theory.

IV. SATURATION OF INTERCHANGE MODES

In this section we discuss the saturation mechanism of the resistive g-modes and compare the theoretically predicted values with the simulation results. There are basically two mechanisms which can saturate the resistive interchange mode. The first mechanism is compressional stabilization, which has been discussed by Manheimer.[20] The idea is that the energy released by the unstable plasma ceases to drive unstable modes and begins to compress the plasma. The resulting saturation level is obtained by balancing the gravitational and compressional energy of a displaced fluid element. This mechanism would predict higher saturation levels because it ignores the damping due to resistive field line bending.

The second mechanism is by convective mixing of pressure or density. This saturation process has been proposed by Carreras et al.[21] to determine the saturation level of resistive ballooning modes. A similar method has been applied to rippling modes[22] where resistivity, rather than pressure, is convected. The latter mechanism of convective mixing of pressure is more plausible since relaxation of the density profile occurs on a much shorter time scale than compressional effects. Furthermore, with narrow layer widths about the

mode rational surface one expects the convection process to be quite rapid.

An estimate of the saturation level can be made by considering the equation for convection of pressure:

$$\frac{\partial p}{\partial t} + \underset{\sim}{v} \cdot \underset{\sim}{\nabla} p = 0 \ . \tag{14}$$

By writing $p = \langle p \rangle + \hat{p}$, $\underset{\sim}{v} = \langle \underset{\sim}{v} \rangle + \hat{\underset{\sim}{v}}$, we obtain an equation for $\hat{p}$:

$$\frac{\partial \hat{p}}{\partial t} + \hat{\underset{\sim}{v}} \cdot \underset{\sim}{\nabla} \langle p \rangle + \hat{\underset{\sim}{v}} \cdot \underset{\sim}{\nabla} \hat{p} = 0 \ , \tag{15}$$

under the assumption $\langle \underset{\sim}{v} \rangle = 0$. Fourier transforming in the y-direction, we obtain an equation for the k=0 component of the perturbed pressure

$$\frac{\partial \hat{p}_o}{\partial t} = -\hat{\underset{\sim}{v}}_k \cdot \underset{\sim}{\nabla} \hat{p}_{-k} - \hat{\underset{\sim}{v}}_{-k} \cdot \underset{\sim}{\nabla} \hat{p}_k \ . \tag{16}$$

Letting $\hat{\underset{\sim}{v}} \simeq \gamma \hat{\underset{\sim}{\xi}}$, where $\underset{\sim}{\xi}$ is the fluid displacement, and $k_x > k_y = k$, we obtain

$$\hat{p}_o = \frac{\partial}{\partial x} |\hat{\xi}_k|^2 \frac{\partial \langle p \rangle}{\partial x} \ , \tag{17}$$

which can be substituted into the equation

$$\frac{\partial \hat{p}_k}{\partial t} + \hat{\underset{\sim}{v}}_k \cdot \underset{\sim}{\nabla} (\langle p \rangle + \hat{p}_o) = 0 \tag{18}$$

to give

$$\hat{p}_k = -\hat{\xi}_k\left(1 - \frac{\partial^2 |\xi_k|^2}{\partial x^2}\right)\frac{\partial \langle p\rangle}{\partial x} \ . \tag{19}$$

Therefore, convection of pressure would cease when

$$|\xi_k|^2 \simeq \Delta_k^2 \ , \tag{20}$$

where Δ_k is the approximate layer width of the mode. The saturation occurs when the pressure fluctuation is displaced by a distance comparable to the width of the eigenmode.

The saturated level can be approximated by assuming convection occurs mainly through $\underset{\sim}{E}\times\underset{\sim}{B}$ motion. Approximating the $\underset{\sim}{E}\times\underset{\sim}{B}$ velocity perturbation by $\hat{v}_x \simeq \gamma\Delta_k$, where γ is the linear growth rate, the fluctuation level of the unstable modes at saturation is given by

$$\frac{e\hat{\phi}_k}{T_e} \simeq \gamma\Delta_k \frac{eB}{k_y T_e} \ . \tag{21}$$

Figure 8 is an illustration of the mode fluctuation amplitude versus time for the most unstable mode, $k_y\rho_s = 0.036$ with $\nu_{ei}/\omega_* = 2000$. From this figure $2\gamma/\omega_{pe} \simeq 0.0004$ and $\Delta/2 \simeq 16$, which gives a value of $e\hat{\phi}/T_e \simeq 0.8$ at saturation using Eq. (21). The measured value is $e\hat{\phi}/T_e \simeq 0.22$. Therefore, the instability saturates at a lower value than predicted by theory. However, the estimate given by Eq. (21) is considered only an upper bound. The simulation values and predictions of Eq. (21) were found for differing values of the resistivity, with

better agreement for the longer wavelengths modes and poor agreement for shorter wavelengths. This is shown in Fig. 9, where we have plotted $e\hat{\phi}/T_e$ versus $(\nu_{ei}/\omega_*)^{2/3}$ for the same value of k_y at saturation.

V. CONCLUSIONS

We have used particle simulation methods to investigate the dynamical evolution of resistive g-modes in a sheared magnetic field. Since the slow modes are very localized about the mode rational surface, on the order of a few ion gyroradii, finite Larmor radius effects as well as diamagnetic drifts are important because they alter the scaling of the growth rates with resistivity. The fast interchange mode is first considered and it is found that several long wavelengths grow at the theoretically predicted values. The modes saturate when the density profile relaxes, thereby nullifying the free energy source for instability.

For the slow interchange modes, corresponding to a growth rate dependence on resistivity to the one-third power, the density profile was observed to quasilinearly flatten over the width of the eigenmode. Several simulations were performed with varying resistivity and it was found that the growth rate obeyed the proper scaling law obtained from linear theory for $\omega > \omega_*$. The presence of magnetic shear introduces a constraint which twists the mode to conform to the field lines and this causes the lowered value of the growth rate.

The saturation of the interchange modes is primarily caused by $\underset{\sim}{E}\times\underset{\sim}{B}$ convection of pressure or density. The plasma is convected across the magnetic field until the perturbed pressure response vanishes, which in

turn saturates the modes. This convection process occurs over the width of the eigenmode. Since the width of the mode for the slow interchange is much smaller than that of the fast, the saturation level is also much less.

With the convection occurring over the mode width, it is expected that in cases of multi-rational surfaces the modes centered about different rational surfaces would interact and produce a turbulent state. Therefore, an extension of this work to three dimensions would be to consider the interaction of modes with different helicities (i.e., different k_z's) and determine the saturated levels as well as the energy transfer in the fluctuation spectrum. Furthermore, when magnetic perturbations are allowed, the overlapping of magnetic islands can occur and the effects of stochastic field lines on transport coefficients in the collisional and collisionless regimes can be investigated.

ACKNOWLEDGMENTS

The authors would like to thank F. Brunel for many helpful discussions. This work was supported by the U.S. Department of Energy, under grant DE-FG05-80-ET-53088 and the National Science Foundation, under grant ATM-82-14730.

REFERENCES

1. H.A.B. Bodin and A.A. Newton, Nucl. Fusion 20, 1255 (1980).

2. M.N. Rosenbluth and M.N. Bussac, Nucl. Fusion 19, 489 (1979).

3. B. Coppi, J.M. Greene, and J.L. Johnson, Nucl. Fusion 6, 101 (1966).

4. H.P. Furth, J.A. Killeen, and M.N. Rosenbluth, Phys. Fluids 6, 459 (1963).

5. T.E. Stringer, Nucl. Fusion 15, 125 (1975).

6. T.E. Stringer, Phys. Fluids 10, 418 (1967).

7. C.L. Chang, N.T. Gladd, and C.S. Liu (to be published).

8. J.M. Finn, W.M. Manheimer, and T.M. Antonsen, Naval Research Laboratory Report #4783 (1982).

9. D.D. Schnack, J.A. Killeen, and R.A. Gerwin, Nucl. Fusion 21, 1447 (1981).

10. T.C. Hender and D.C. Robinson, Nucl. Fusion 21, 755 (1981).

11. T.C. Hender and D.C. Robinson, Computer Phys. Comm. 24, 413 (1981).

12. T.C. Hender and D.C. Robinson, in Plasma Physics and Controlled Nuclear Fusion Research (International Atomic Energy Agency, Vienna, 1983), Vol. 3, p. 417.

13. Z.G. An and P.H. Diamond, Sherwood Theory Meeting, Arlington, Virginia, 1983, paper 2523.

14. N.R. Ainsworth, M.W. Alcock, R.E. Bradford, P.R. Collins, J.G. Gordey, T. Edlington, W.H.W. FLetcher, E.M. Jones, M.F. Payne, A.C. Riviere, D.F.H. Start, C.A. Steed, D.R. Sweetman, and T.N. Todd, in Plasma Physics and Controlled Nuclear Fusion Research (International Atomic Energy Agency, Vienna, 1978), Vol. 1, p. 745.

15. A.J.L. Venhage and D.C. Robinson, Pulsed High Beta Plasma, edited by D.E. Evans (Pergamon Press, Oxford, 1975), p. 267.

16. W.W. Lee and H. Okuda, J. Comp. Phys. 26, 139 (1975).

17. R. Shanny, J.M. Dawson, and J.M. Greene, Phys. Fluids 10, 1281 (1967).

18. C.Z. Cheng and H. Okuda, J. Comp. Phys. 25, 133 (1977).

19. A.B. Mikhailovskii, Theory of Plasma Instabilities, Vol. 2, Chap. 9 (Consultants Bureau, N.Y., 1974).

20. W.M. Manheimer, Phys. Rev. Lett. 45, 1249 (1980).

21. B.A. Carreras, P.H. Diamond, M. Murakami, J.L. Dunlap, J.D. Bell, H.R. Hicks, J.A. Holmes, E.A. Lazarus, V.K. Paré, P. Similon, C.E. Thomas, and R.M. Wieland, Phys. Rev. Lett. 50, 503 (1983).

22. B.A. Carreras, P.W. Gaffney, H.R. Hicks, and J.D. Callen, Phys. Fluids 25, 1231 (1982).

FIGURE CAPTIONS

Fig. 1 Initial configuration for particle simulation model.

Fig. 2 Fast interchange mode case. Theory and simulation values of growth rate versus wavenumber.

Fig. 3 Fast interchange mode case. Contours of the electrostatic potential taken at time $\omega_{pe}t = 1600$. Distances normalized to ρ_s and solid curves are positive potential and dotted curves represent negative potential.

Fig. 4 Fast interchange mode case. Plot of mode amplitude at saturation versus wavenumber.

Fig. 5 Slow interchange mode case. Time evolution of the electron and ion density profiles. The profiles illustrated are chosen at $\omega_{pe}t = 0$ and $\omega_{pe}t = 3600$, near saturation. The theoretically determined eigenmode width, Δ, is also shown in this figure.

Fig. 6 Numerically obtained wave function using a standard shooting code method for $\nu_{ei}/\omega_* = 50$ and $k_y\rho_s = 0.036$. Δ refers to the half-width of the eigenmode wave function.

Fig. 7 Slow interchange mode case. Simulation and theoretical values (solid line) of growth rate versus resistivity to the one-third power for modes $k_y\rho_s = 0.012$ and 0.036.

Fig. 8 Slow interchange mode case. Mode amplitude versus time for $\nu_{ei}/\omega_* = 2000$ and $k_y\rho_s = 0.036$. Dotted line represents linear theory growth rate.

Fig. 9 Slow interchange mode case. Mode amplitude at saturation versus resistivity to the two-thirds power. The solid line is the mixing length theory prediction.

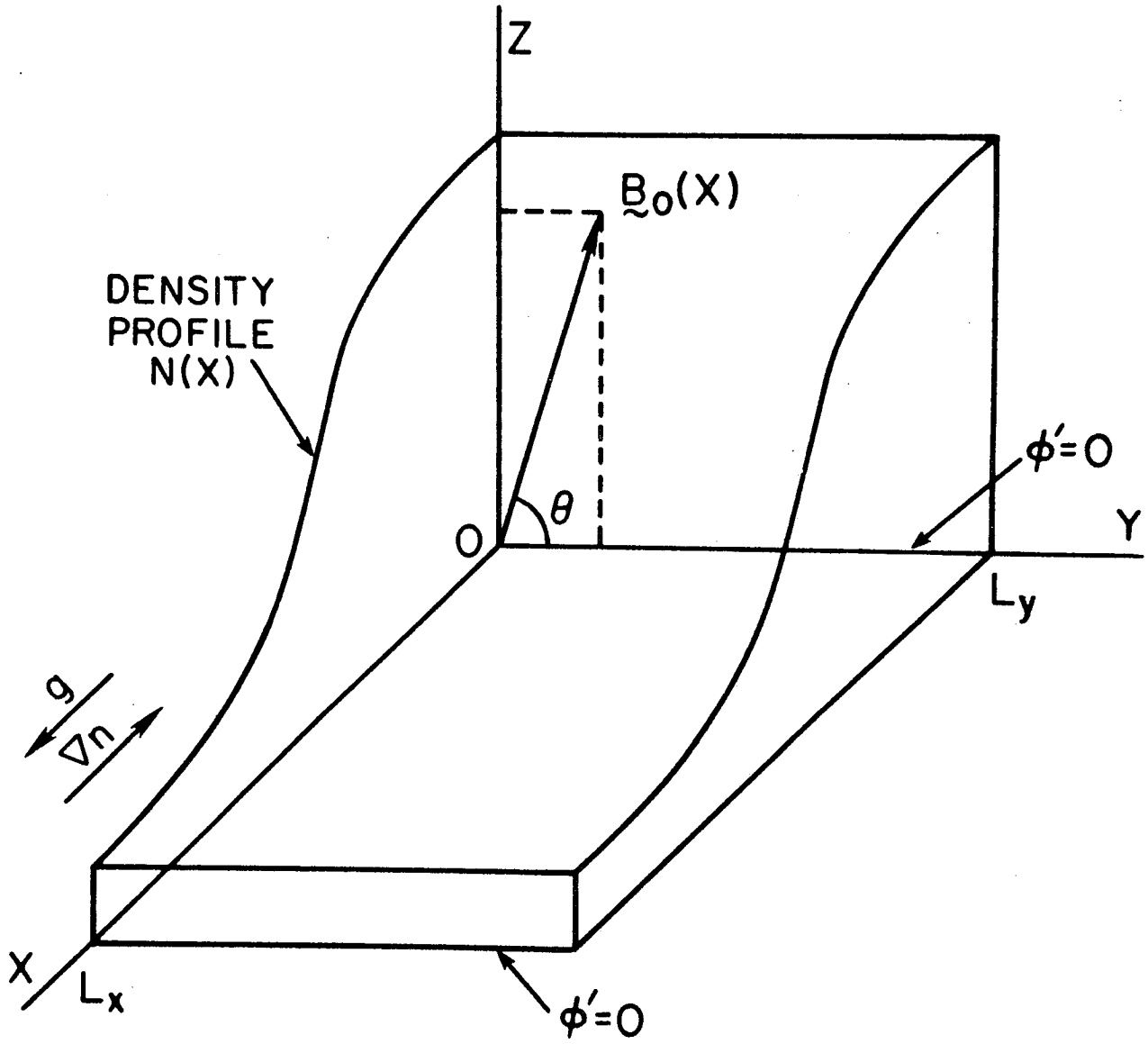
Z
$\underset{\sim}{B}_0(X)$
DENSITY
PROFILE
N(X)
$\phi'=0$
θ
O
Y
L_y
g
∇n
X
L_x
$\phi'=0$

Fig. 1

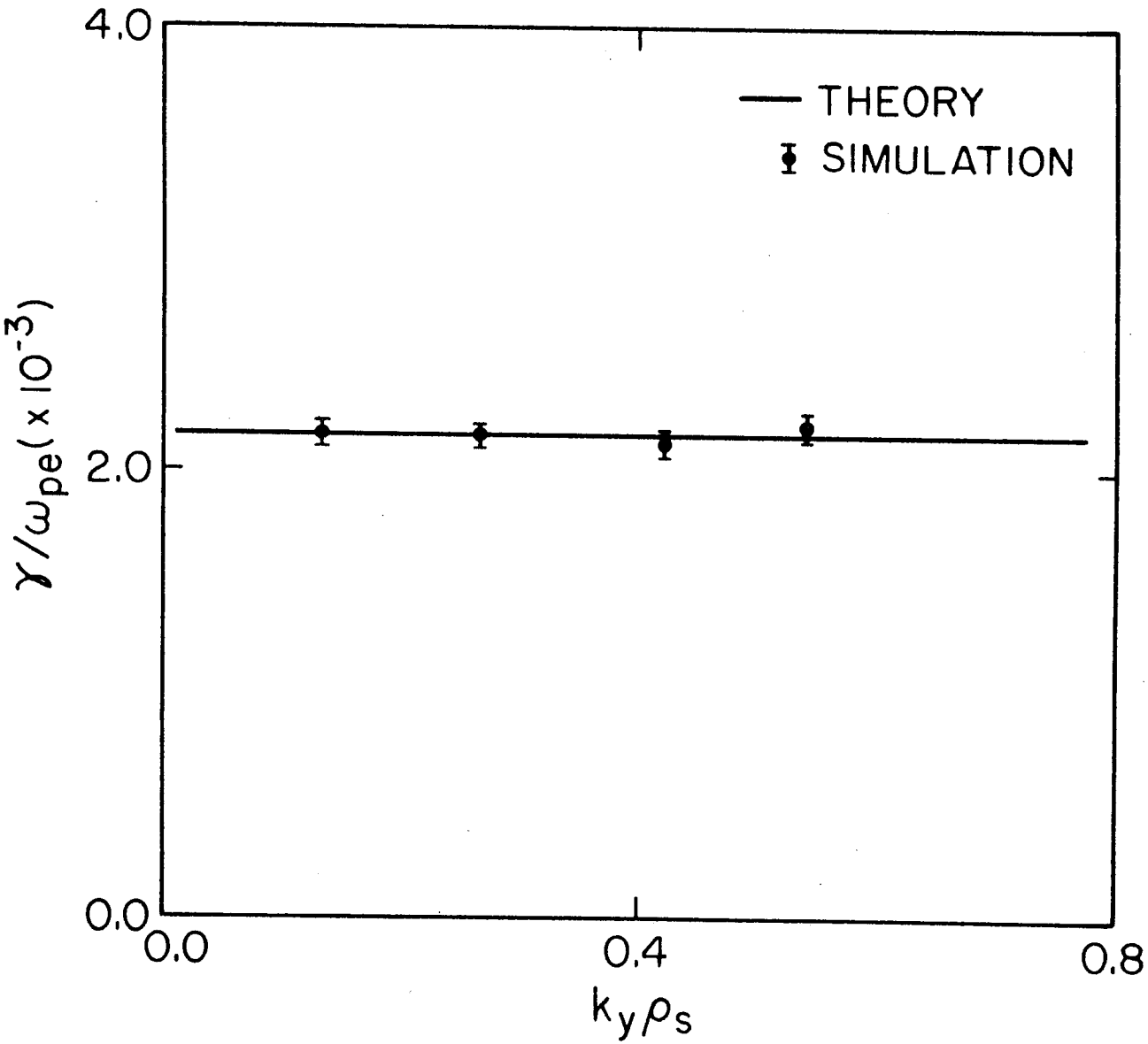
4.0
2.0
0.0
0.0
0.4
0.8
THEORY
SIMULATION
$\gamma/\omega_{pe}(\times 10^{-3})$
$k_y\rho_s$

Fig. 2

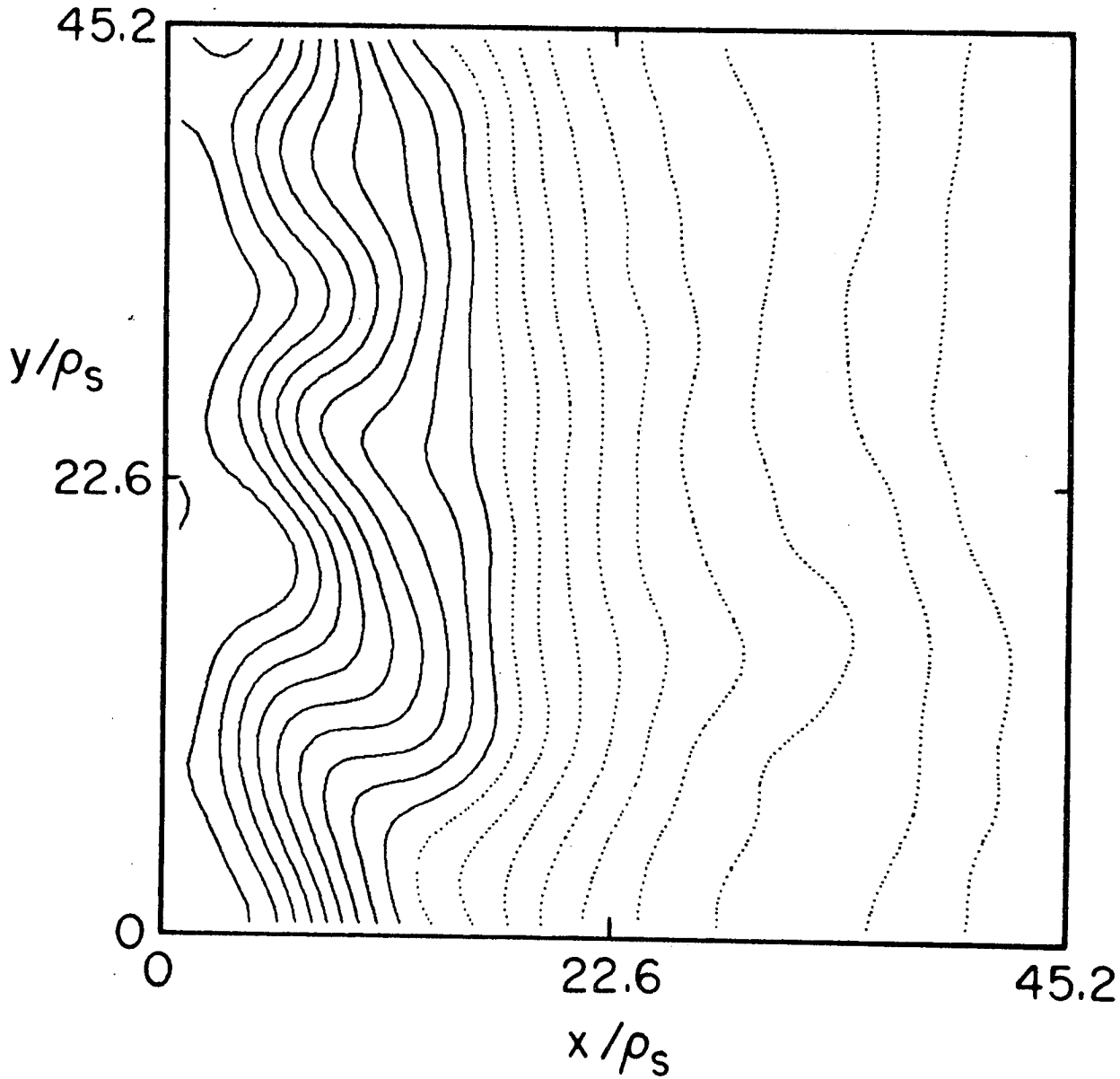

Fig. 3

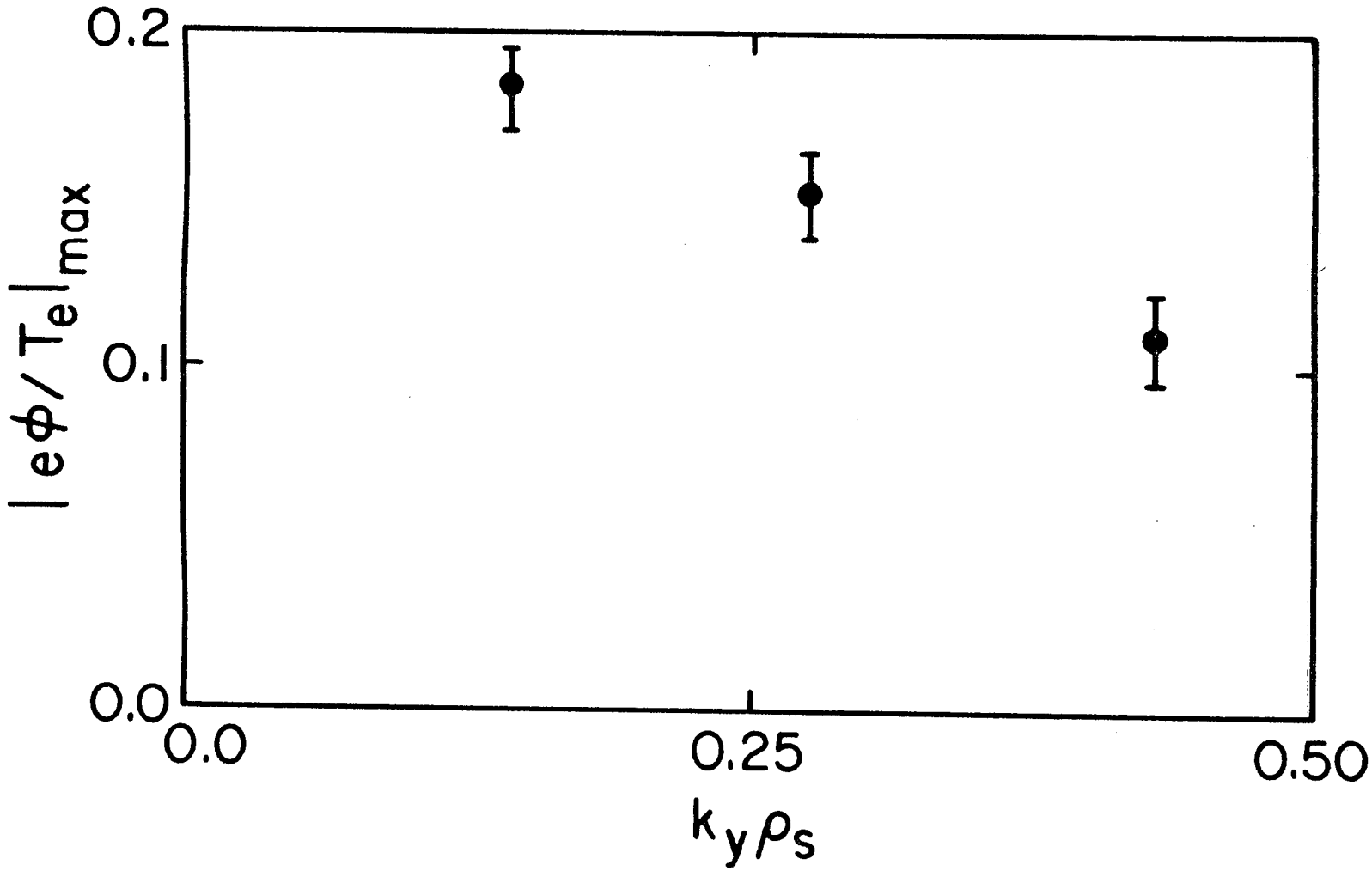

Fig. 4

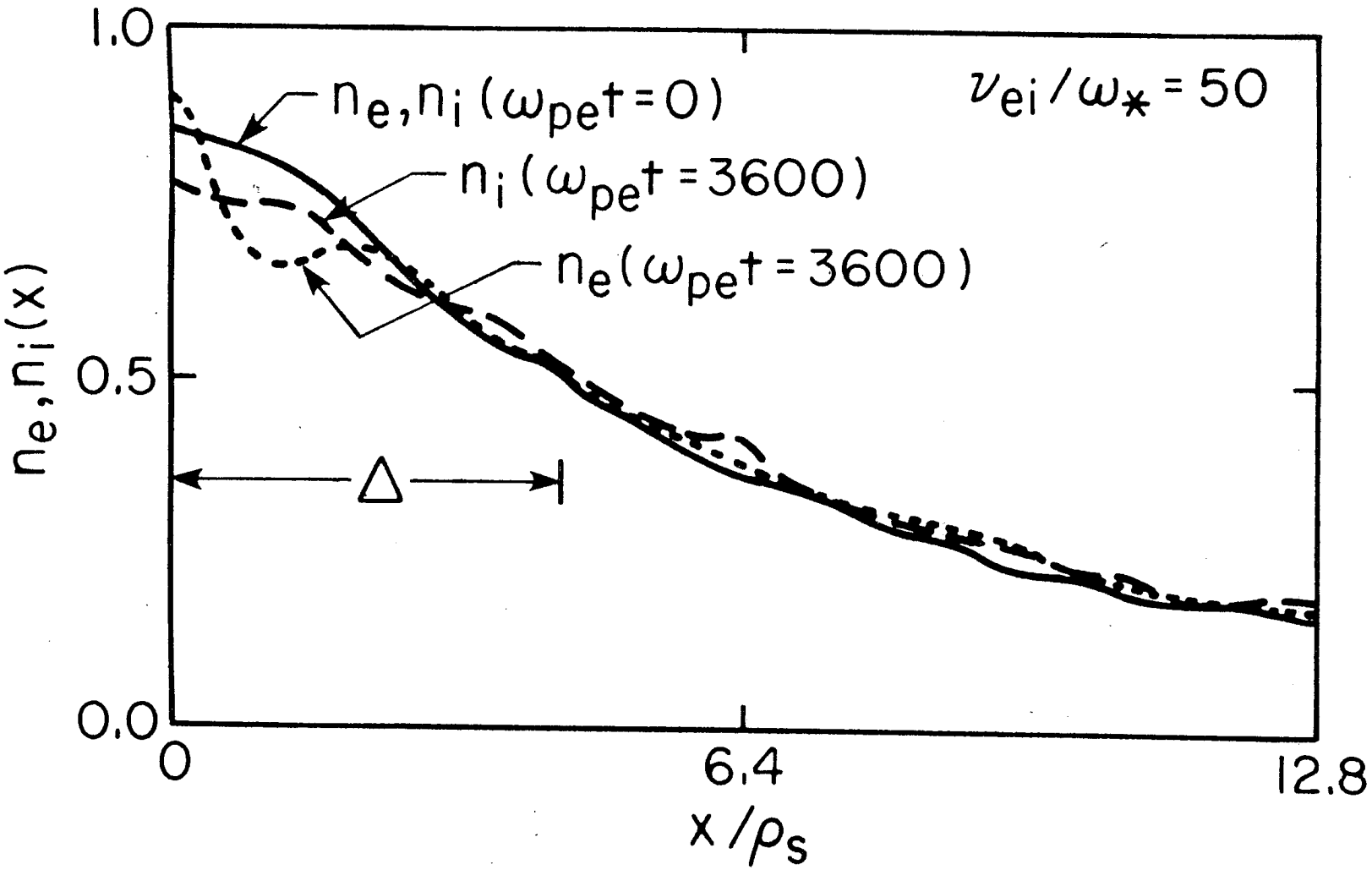
1.0
0.5
0.0
0
6.4
12.8
$n_e, n_i(x)$
x/ρ_s
$n_e, n_i\ (\omega_{pe}t = 0)$
$n_i\ (\omega_{pe}t = 3600)$
$n_e\ (\omega_{pe}t = 3600)$
$\nu_{ei}/\omega_* = 50$
Δ

Fig. 5

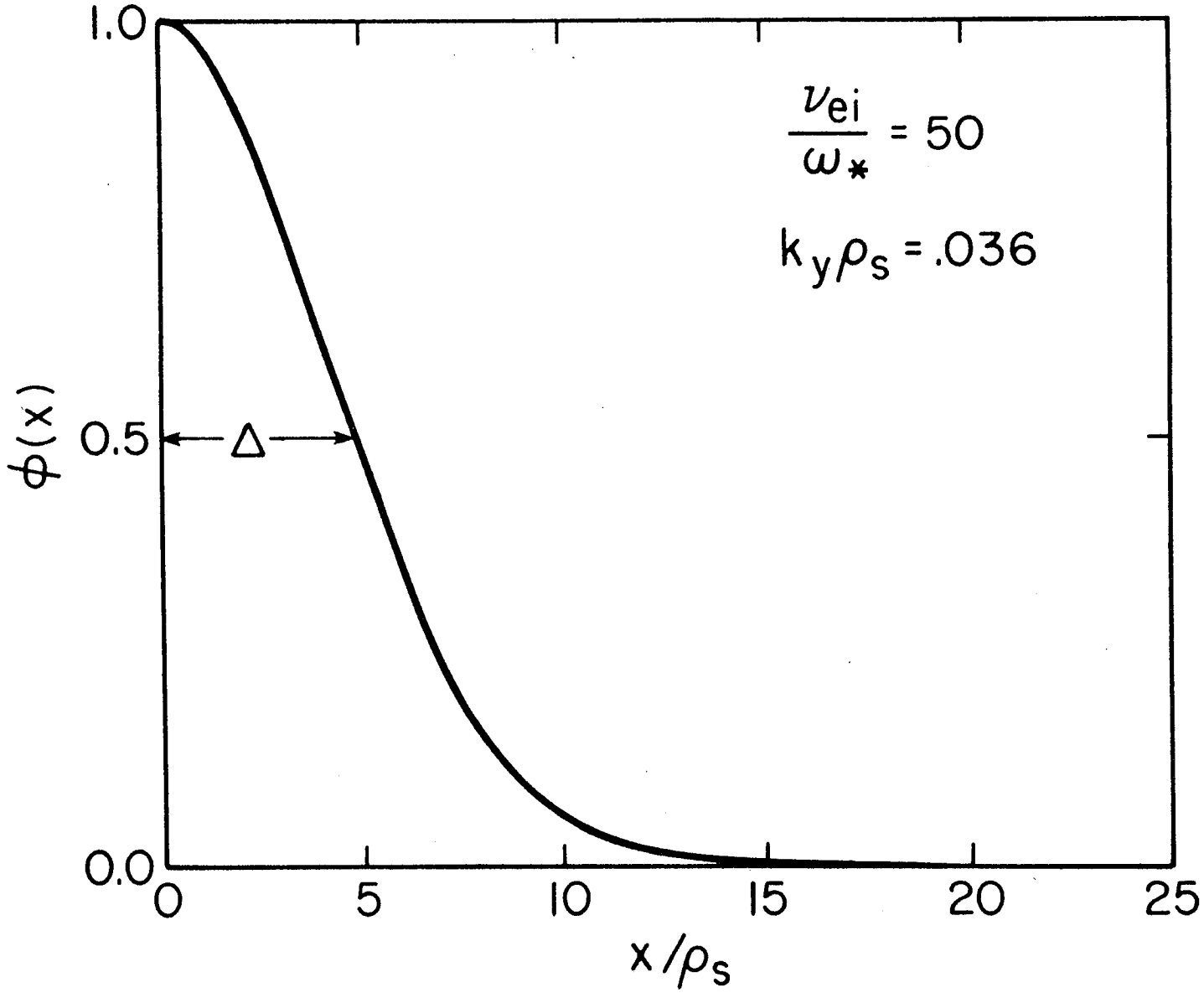
1.0
0.5
0.0
$\phi(x)$
$\frac{\nu_{ei}}{\omega_*} = 50$
$k_y\rho_s = .036$
Δ
0
5
10
15
20
25
x/ρ_s

Fig. 6

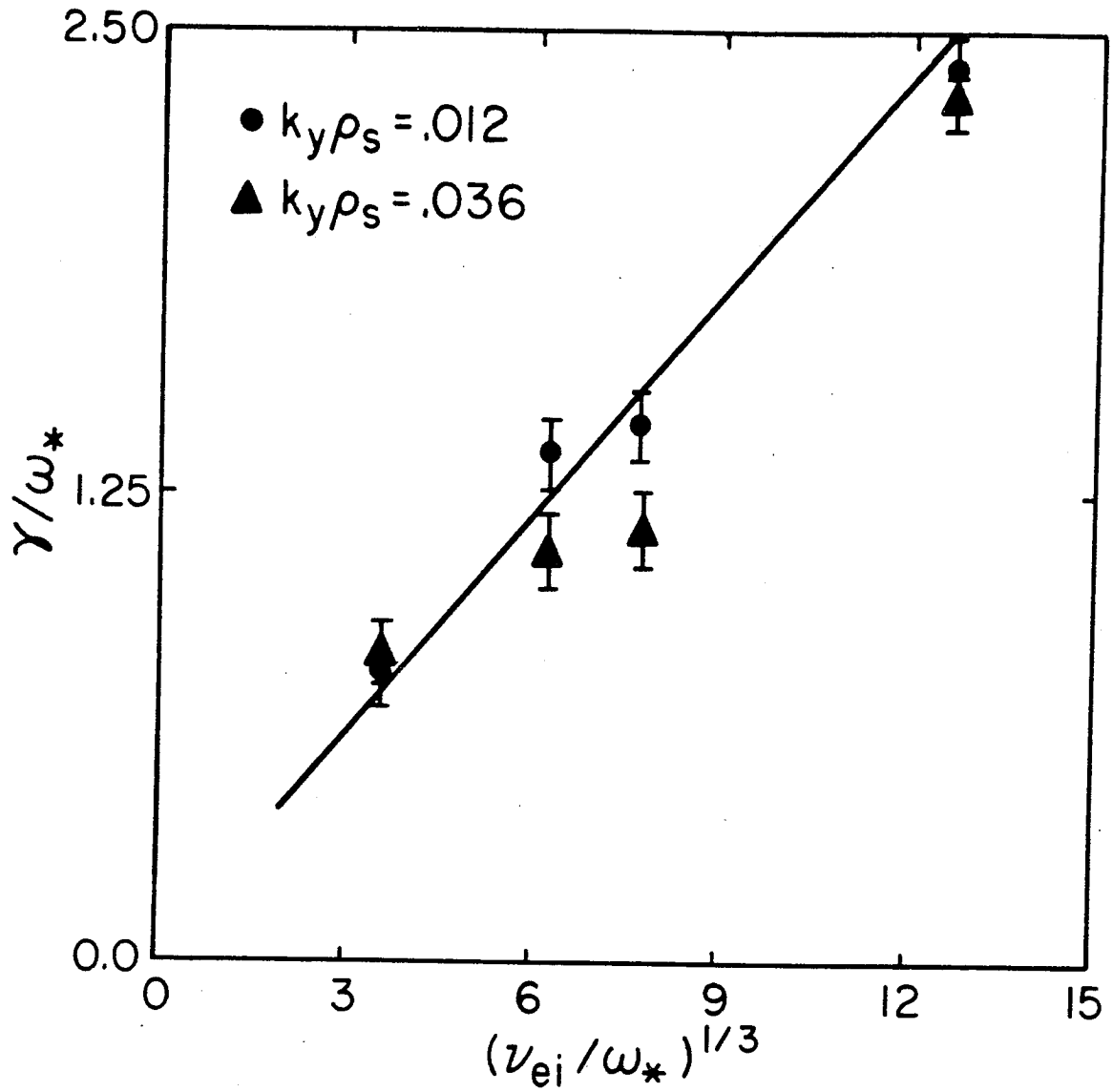
2.50
1.25
0.0
γ/ω_*
$k_y\rho_s = .012$
$k_y\rho_s = .036$
0
3
6
9
12
15
$(\nu_{ei}/\omega_*)^{1/3}$

Fig. 7

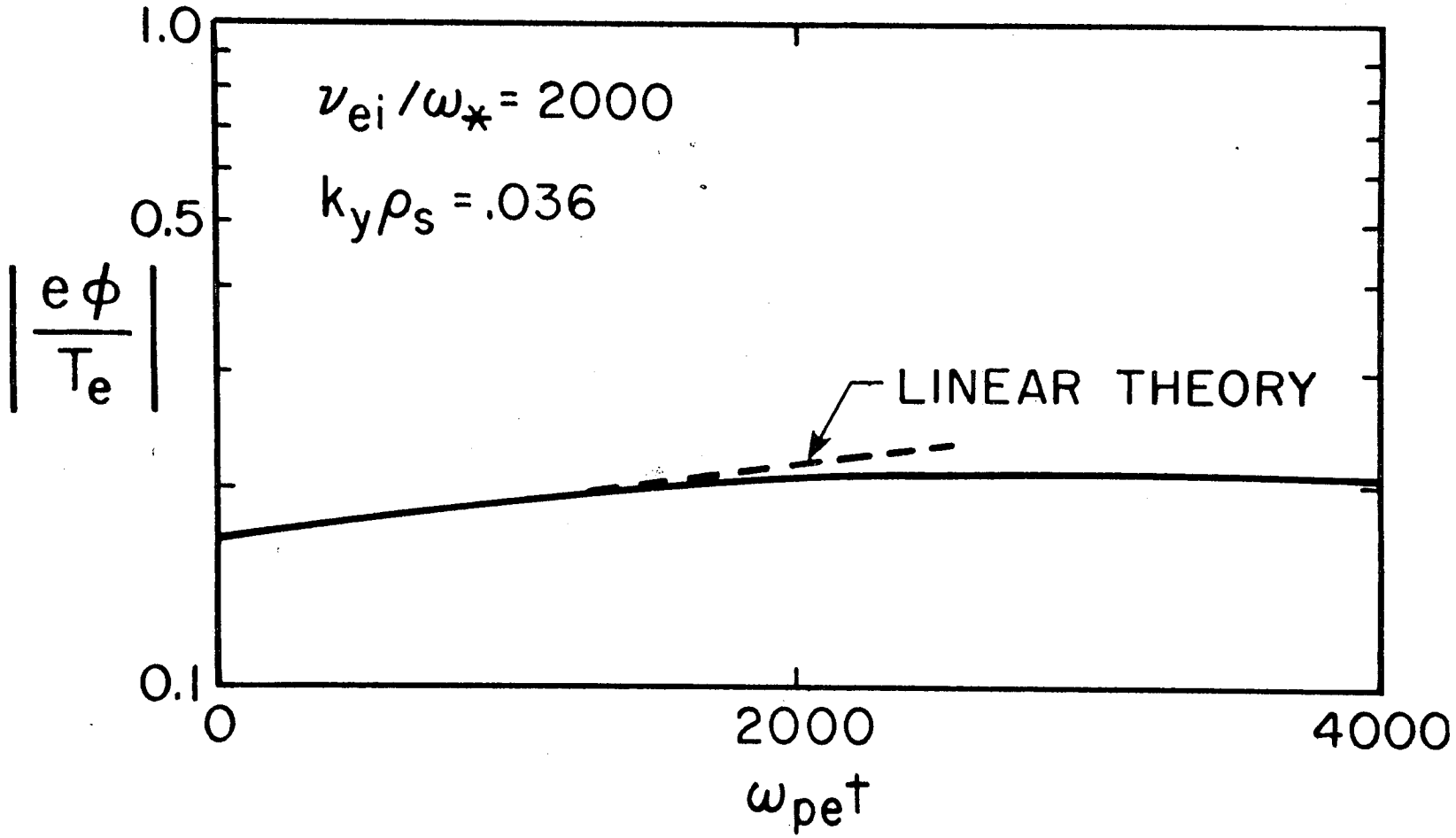
1.0
0.5
0.1
$\nu_{ei}/\omega_* = 2000$
$k_y\rho_s = .036$
$\left|\frac{e\phi}{T_e}\right|$
LINEAR THEORY
0
2000
4000
$\omega_{pe}t$

Fig. 8

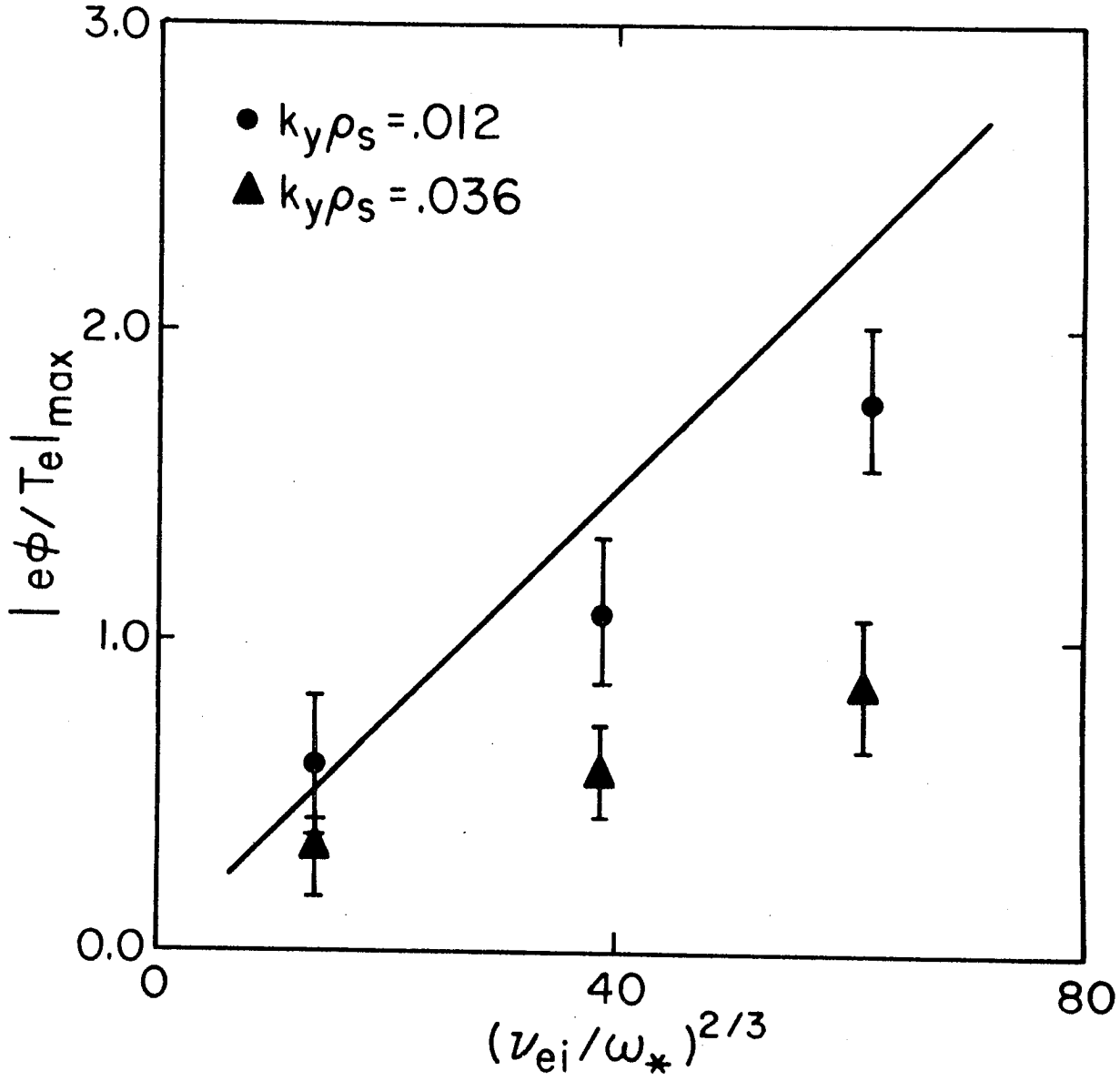
3.0
2.0
1.0
0.0
0
40
80
$|e\phi/T_e|_{max}$
$(\nu_{ei}/\omega_*)^{2/3}$
$k_y\rho_s = .012$
$k_y\rho_s = .036$

Fig. 9